Scientific Reports

https://doi.org/10.1038/s41598-026-45527-9

Article in Press

Prevention measures and monitoring technology of dynamic load in Tangshan coal mine after coal bump disaster

Received: 7 November 2025

Accepted: 19 March 2026

Published online: 23 March 2026

Cite this article as: Ma S., Su Y., Jia D. *et al.* Prevention measures and monitoring technology of dynamic load in Tangshan coal mine after coal bump disaster. *Sci Rep* (2026). https://doi.org/10.1038/s41598-026-45527-9

Shuangwen Ma, Yang Su, Dongxu Jia, Xin Wang, Guanghan Li, Baolong Guo, Haina Li & Tao Wu

Prevention Measures and Monitoring Technology of Dynamic Load in Tangshan Coal Mine after Coal Bump Disaster

Shuangwen Ma[1,2,3,4 *], Yang Su[2,3,4], Dongxu Jia[2,3,4], Xin Wang [2,3,4], Guanghan Li [2,3,4], Baolong Guo [2,3,4], Haina Li [2,3,4], Tao Wu [5]

1. *Ordos Research Institute, Liaoning Technical University, Ordos, Inner Mongolia, 017004, China*

2. *College of Mining Engineering, Liaoning Technical University, Fuxin 123000, China*

3. *Research Center of Coal Resources Safety Mining and Clean Utilization，Fuxin 123000，China*

4. *Collaborative Innovation Center of Mine Major Disaster Prevention and Environmental Restoration, Fuxin 123000, Liaoning, China*

5. *Kaiyuan Narinxili Coal development Co., LTD, Ordos, Inner Mongolia, 017206, China*

** Correspondence email: maswen3935@163.com*

ABSTRACT

Coal bumps pose a significant threat to the safe operation of coal mines. This study examines the coal bumps incident at Tangshan Mine, focusing on the influences of various disaster-causing factors, including structural stress, rock mass impact tendencies, and support and bearing capacity. To facilitate the safe resumption of production at the 0250 working face, coal seam blasting and borehole pressure relief drilling were conducted to dissipate the accumulated elastic energy within the coal seam, thereby effectively mitigating the risk of bursting. Concurrently, the vibration and displacement of the roof were monitored. The relevant monitoring data indicate that roof activity remains within a controllable range, suggesting a relatively low likelihood of coal bump incidents.

Keyword: Coal bump; Monitoring Technology; Vertical Velocity;

1 Introduction

Coal bumps are dynamic phenomena resulting from the sudden release of elastic deformation in coal bodies during mining operations. These events are destructive and can trigger additional geo-disasters, making them one of the most severe hazards in coal mining. On October 20, 2018, a coal bump at the Longyun coal mine led to 21 fatalities. Similarly, a coal bump at the Longjiabao coal mine on June 9, 2019, resulted in 9 deaths. As underground resource exploitation progresses, coal bumps have significantly hindered deep mining, presenting a critical challenge for the coal mining industry [1-4].

On August 2, 2019, a major coal bump occurred at the Tangshan coal mine, causing 7 deaths. Investigative findings indicate that the causes of coal bump incidents can be attributed to four factors: (1) Geological factors reveal that the geological structure of the Tangshan coalfield is complex, with elevated tectonic stress. (2) The mechanical properties of the surrounding rock show that both the coal seam and the roof of the working face exhibit a weak tendency for impact. (3) Regarding static load concentration, peninsula coal pillars formed in the accident area after the surrounding coal seam was mined, resulting in relatively high abutment pressure. (4) Dynamic load factors indicate that mining activities disturb the coal rock structure.

Following the accident investigation, the Tangshan coal mine is undergoing a feasibility analysis for resuming production. Resumption of mining operations can only occur if appropriate preventive measures are implemented to eliminate and mitigate factors that induce bursts, thereby ensuring safety conditions in the burst-prone mining area. The feasibility of resuming production can be assessed through four key aspects. First, geological factors represent natural elements that contribute to high ground pressure and geological disasters[5-8]. Tectonic stress serves as a primary force behind certain geological disasters, including coal bumps [5-15]. Additionally, gas content and water seepage are linked to geological hazards[16-19]. Geological structures, such as faults and folds, can lead to stress concentration or abrupt changes in geological conditions, making them significant contributors to geological disasters[20-25]. The inherent nature of geological factors is challenging to modify on a large scale. To reduce static load stress concentration, mining deployment will be optimized, and the stress concentration associated with the peninsula briquette pillar will be alleviated. In response to the impact tendencies of the coal mass, blasting of the coal body and pressure relief drilling will be conducted. Following evaluation, it has been determined that mining operations can proceed; however, monitoring of mining disturbances will be essential throughout the mining process.

The monitoring and early warning of dynamic pressure disturbances remain a significant challenge in the study of coal bumps. Unlike other monitoring parameters such as water, fire, gas, and dust, dynamic disturbances are not physical phenomena and cannot be directly observed. Consequently, monitoring these disturbances through parameterization presents a considerable challenge. Currently, commonly employed methods for monitoring dynamic disturbances include drilling power, energy accumulation (EA), stress monitoring, electromagnetic techniques, microseismic detection, and the recently developed computed tomography (CT) monitoring technology. Although these technologies have found extensive application in engineering practice, their indirect nature results in non-intuitive data and complicates analysis. Furthermore, some methods measure the cumulative effects of dynamic and static loads, making it difficult to isolate the contribution of dynamic loads. Therefore, developing a novel method for the direct monitoring of the movement of the front roof under dynamic load disturbances is of paramount importance.

This paper focuses on the dynamic disturbance monitoring of the 0250 working face at the Tangshan coal mine. It introduces a vibration instrument utilized in the machinery industry and slope monitoring to directly observe the movement of the roof in front of the working face during mining operations. By integrating roof subsidence monitoring, the study analyzes the movement of the roof under static stress and

the effects of dynamic disturbances on the coal and rock mass structure, thereby ensuring the safe production of the 0250 working face. This research offers a novel monitoring approach for assessing mine dynamic loads and provides new technical means for predicting impact ground pressure. The monitoring data serve as a reference for the dynamic load analysis of similar mining operations.

2 Engineering background

The Tangshan coal mine is located in the southwest region of the northwest wing of the Kaiping coalfield, with an annual production capacity of 4.2 million tons. The mine field contains eight mineable seams, specifically seams 5, 8, and 9. The geological structure of the mine field is intricate, as illustrated in Figure 1, with the primary structures being the FI and FV faults. The FV fault serves as the boundary of the mine field, with an elevation exceeding 500 meters. This mining area is part of the Yuegezhuang wave fold belt and is intersected by the FV fault in the southeast. Based on mining exposure, there are 16 faults designated as f1 through f16 within the mining area.

The buried depth of 0250 working face is 697-835 m, the inclined length is 150m, and the strike length is 568m. The south of the working face is the y257 roadway, the East is the 0251 goaf, the north is the 8241, 8242, 8250 roadway, and the west is the coal transportation system, as shown in Figure 2. The stoping line of working face is the fold axis.

The buried depth of the 0250 working face ranges from 697 to 835 m, with an inclined length of 150 m and a strike length of 568 m. To the south of the working face lies the y257 roadway, while the 0251 goaf is located to the east. The north is bordered by the 8241, 8242, and 8250 roadways, and the coal transportation system is situated to the west, as illustrated in Figure 2. The stopping line of the working face corresponds to the fold axis.

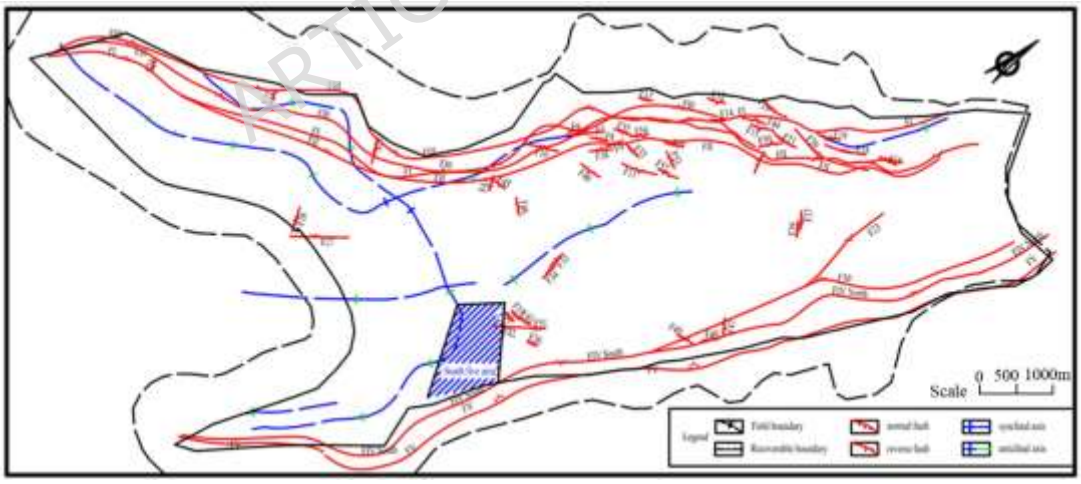

Figure 1. Geological structure of Tangshan mine and study area.

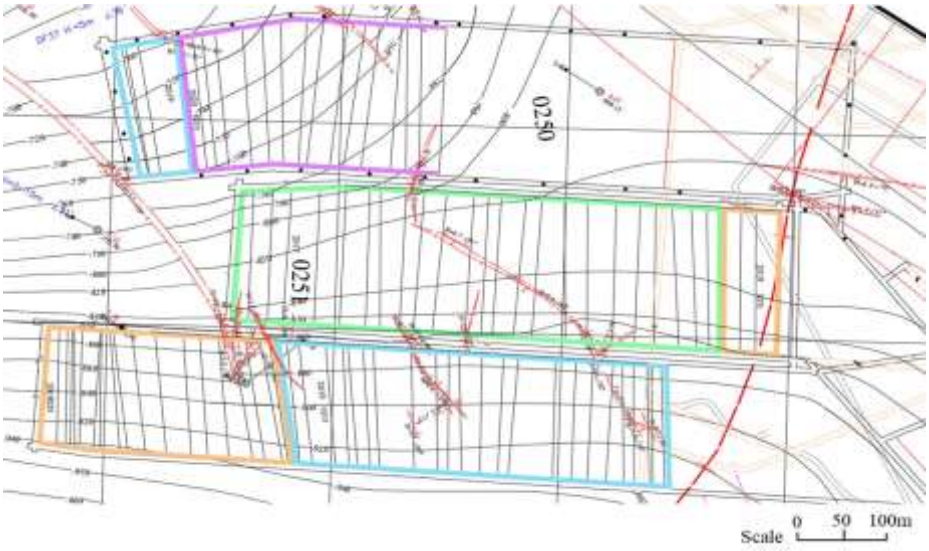

Figure 2. The studied area.

The coal seam at the 0250 working face exhibits a dip angle ranging from 4° to 35°, with an average dip angle of 20°. The coal thickness varies between 1.8 m and 3.9 m, yielding an average thickness of 2.8 m. The coal quality is characterized by low ash and low sulfur content. Regarding bearing capacity, physical and mechanical test results indicate that the uniaxial compressive strength (UCS) of the coal sample is 11.1 MPa, while the tensile strength measures 0.67 MPa. The immediate roof consists of mudstone with a thickness of 0.2 m to 0.6 m, exhibiting an average UCS of 22.3 MPa. The main roof is composed of siltstone, with an average thickness of 5.7 m and an average UCS of 115 MPa. A comprehensive histogram of the 0250 working face is presented in Figure 3.

During the development of the roadway, eight faults were identified: 0250-f1 measuring 1.4 m, 0250-f2 at 2.9 m, 0250-f3 at 2.0 m, 0250-f4 at 0.9 m, 0250-f5 at 5.5 m, 0250-f6 at 3.8 m, 0250-f7 at 0.9 m, and 0250-f8 at 3.0 m. Overall, the stability of the mining roadway is satisfactory; however, the presence of faults and a weak immediate roof adversely affects mining operations and coal quality.

3 Burst prevention flow chart

On August 2, 2019, a significant coal bump incident transpired at the Tangshan coal mine, leading to the deaths of seven individuals. The underlying cause of the coal bump is attributed to a complex interplay of geological factors, the properties of surrounding rock, abutment pressure, and dynamic disturbances. The flow chart for burst prevention is illustrated in Figure 4.

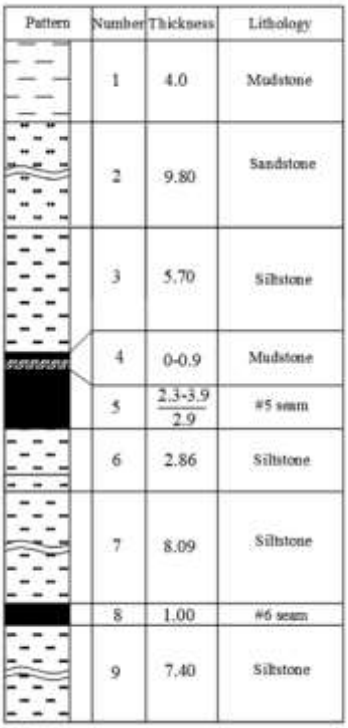

Figure 3. Comprehensive geological histogram of 0250 working face.

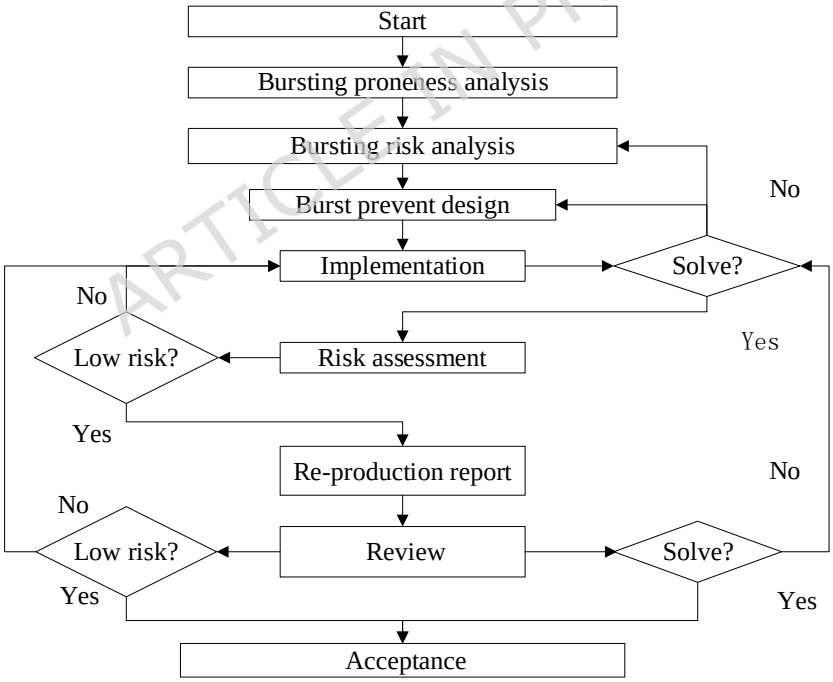

Figure 4. The burst prevention flow chart.

The surrounding rock of coal seam 5 exhibits a weak tendency for impact. In terms of burst prevention measures, the working face of the mining area is first deployed and optimized to mitigate the abutment pressure exerted by the surrounding goaf on the working face. Despite this optimization, the evaluation of burst proneness at the 0250 working face remains at a medium risk level. Consequently, prior to the commencement of mining at 0250, it is essential to implement pressure release measures to diminish the burst risk to a weak or negligible level. In instances of weak burst proneness, dynamic load monitoring

should be conducted to assess the effects of mining-induced disturbances on the surrounding rock structure, thereby eliminating potential hazards and ensuring safe production.

Pressure relief through rib hole drilling constitutes a primary burst control measure in the Tangshan coal mine. The borehole is designed with a diameter of 108 mm and a depth of 8 m, positioned 0.5 meters above the floor. Although crawler drilling machines are employed for this task, the drilling schedule lacks a stringent definition due to the absence of a theoretical guideline. Consequently, it is essential to investigate the pressure relief procedure associated with the drilling hole to enhance mining safety and optimize the economic viability of the 0250 working face.

4 Pre-mining prevention measures

The burst risk of 0250 working face is medium, so, coal blasting and borehole pressure relief are adopted to reduce the impact risk. The construction scheme is as follows.

4.1 Coal seam blasting

Coal seam blasting serves as a method to alleviate stress concentration. The steps for implementing blasting are as follows: (1) The stress within the coal body is assessed using the drilling powder method, whereby multiple coal powder boreholes are drilled at locations identified as having burst risk to delineate the risk area. (2) Blasting is conducted in the high-risk area. (3) Following the blasting, the coal powder from the drilling holes is analyzed to evaluate the effectiveness of the blast in the vicinity of the blasting hole. If the quantity of pulverized coal is below the critical threshold, it is determined that the coal seam has achieved the desired unloading effect; otherwise, secondary unloading blasting is performed.

The 0250 working face employs a single-row coal seam blasting scheme, as illustrated in Figure 5. In this blasting operation, each cartridge weighs 300 g and measures 300 mm in length. The charge per hole consists of 10 to 15 cartridges, with a minimum of two detonators required for each hole. Additionally, the sealing length must be no less than one-third of the total hole depth. The construction area extends 15 m in front of and 15 m behind the hazardous zone. The first borehole is positioned 15 m from the beginning of the hazard area, with a spacing of 5 m, a depth ranging from 12 to 15 m, and a diameter of Φ 42 mm. The boreholes are aligned along the roadway, maintaining a distance of 0.5 m to 1.5 m from the floor.

4.2 Pressure relief drillings

Large diameter borehole drilling serves as a pressure relief measure aimed at mitigating or delaying the onset of stress. This technique relies on the phenomenon of drilling impact during the drilling process. When drilling occurs near a high-stress zone, energy accumulates in the coal, resulting in a high frequency of drilling impacts and a significant increase in the amount of pulverized coal. Following the drilling operation, a fracture zone develops around the borehole. The borehole gradually collapses, and the proximity of the fracture areas facilitates the breaking of the coal seam, thereby relieving pressure. Borehole pressure relief utilizes the elastic energy stored in the coal seam to fracture the surrounding coal, releasing energy and reducing the risk of a burst under conditions of elevated ground stress.

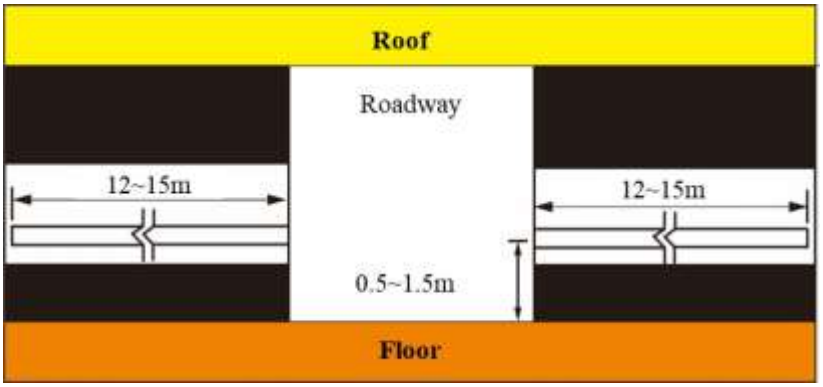

(a)

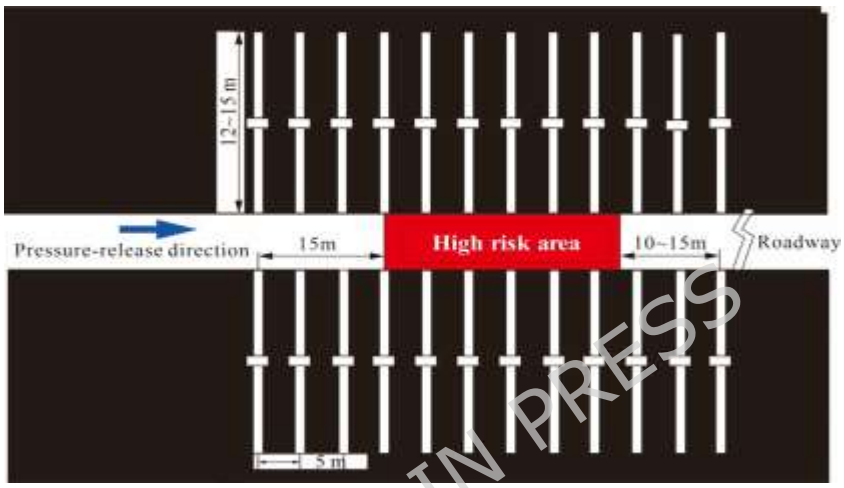

(b)

Figure 5. Layout of coal seam blasting. (a) Front view. (b) vertical view

The drilling pressure relief working range at the 0250 working face matches that of coal blasting, extending 15 m in the burst hazardous zone, as well as 15 m ahead and 15 m behind it. The drilling spacing does not exceed 1 m, with a minimum hole depth of 20 m and a diameter of Φ110 mm. Boreholes are positioned parallel to the coal seam dip, maintaining a distance of 0.5-1.5 m from the floor. If the initial drilling does not mitigate the risk of impact, additional drilling is conducted until the risk is resolved. Refer to Figure 6 for details of the drilling operation.

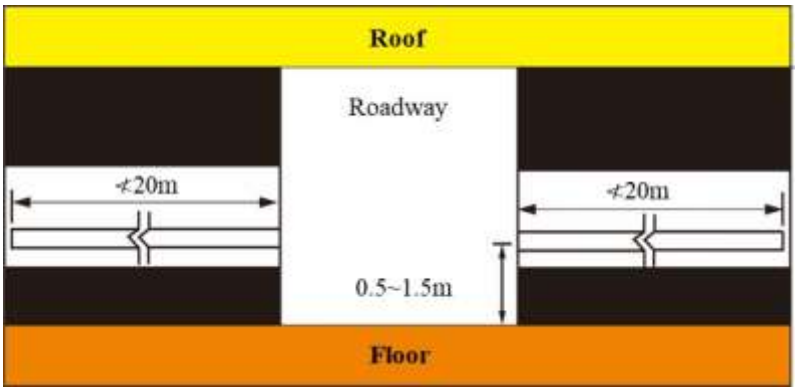

(a)

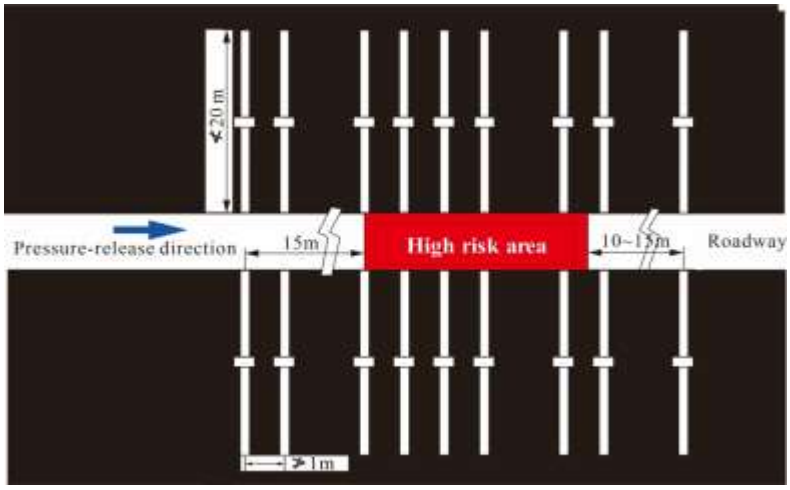

(b)

Figure 6. Layout of drilling holes. (a) Front view. (b) vertical view.

Following coal blasting and borehole pressure relief, the burst risk at the 0250 working face has been diminished to a low level. During the mining process, it is essential to conduct dynamic load monitoring, and additional measures should be implemented as needed to ensure mining safety.

5 Monitoring arrangement

Roof movement induced by mining is a critical factor in the occurrence of coal bumps. The challenge of effectively monitoring and predicting this movement through technological means has long been a concern in coal bump prevention. The drilling powder method serves as an empirical approach, yet it is highly sensitive to geological conditions. The monitoring results of support shield resistance at the working face represent the sum of dynamic and static composite loads. However, the borehole stress meter installed in the roadway rib can only capture relative values, rather than absolute measurements, leading to poor data continuity and significant deviations. Consequently, a discrepancy exists between the monitoring data and actual roof movement, with false positives emerging as a significant issue.

In this study, the TC-4850 vibration meter is employed for the first time to monitor roof movement at various working face advance distances, including the velocity vector and vertical displacement. By integrating these measurements with roof subsidence monitoring data, the analysis of roof movement under dynamic stress is conducted to ensure the mining safety of the 0250 working face.

5.1 Instruments

Tc-4850 is a vibration monitor utilized in the machinery industry and for slope monitoring. The instrument comprises a sensor, a collector, and a connecting cable, as illustrated in Figure 7. The relevant parameters of this instrument are shown in Table 1. The TC-4850 Vibrometer operates by converting vibration waves into voltage signals via its sensor. The conditioned analog electrical signal is then fed into a high-precision A/D conversion module, which converts the continuous analog signal into discrete digital signals. The probe has dimensions of 66 mm on each side. By employing various sensors, it is capable of recording dynamic data, including acceleration, velocity, displacement, and pressure.

Table 1. The relevant of TC-4850 Vibrometer

TC-4850 Vibrometer	
Number of channels:	Parallel three channels
Display mode:	Full Chinese LCD display
Power supply mode:	Rechargeable lithium battery power supply
Sampling rate:	1 kHz ~ 50 kHz, multi-range adjustable
A/D resolution:	16 bit
Frequency response range:	0 kHz to10 kHz
Recording method:	Continuous trigger record, 128 to 1000 times can be recorded
Recording time:	Adjustable in the range of 1 second to 160 seconds
Trigger mode:	Internal trigger or external trigger
Range:	Adaptive range, no setting required, maximum input value 10 V (35 cm/s)
Trigger level:	0 V to 10 V (0 cm/s to 35cm/s) can be adjusted arbitrarily
Storage capacity:	1MB SRAM, 128 MB flash
Recording accuracy:	0.01cm/s
Reading accuracy:	1 ‰
Clock accuracy:	≤ 5 seconds / month
Transmission mode:	USB 2.0
Battery life:	≥ 60 hours
Adapt to the environment:	-10 ℃ to 75 ℃, 0 % to 95 % RH
Size:	168mm × 99mm × 64mm
Weight:	1Kg

Figure 7. TC-4850 vibrometer.

To analyze roof displacement, the SDAK-20 multi-point displacement meter is utilized to monitor changes during vibration assessments. The sensor is installed through roof drilling, with a depth of 10 m and a diameter of 42 mm, achieving a measuring point density of 30 to 500 mm. Figure 8 illustrates the schematic diagram of roof separation monitoring and the corresponding field installation.

Figure 8. SDAK-20 multi-point displacement meter and field installation. (a) Monitoring arrangement. (b) Sensor. (c) Field work.

5.2 Monitoring layout

High stress can easily induce coal bumps in the 0250 working face. Based on mining experience, the influence range of advance abutment pressure at the 0250 working face is estimated to extend approximately 0-33 meters ahead. This range consists of a pressure surge area (3-13 meters), a pressure slow rise area (13-22 meters), a pressure slow decrease area (22-33 meters), and a stable area (beyond 33 meters). The peak position of the pressure is located roughly 22 meters in advance.

The monitoring location is selected in the tailgate of the 0250 working face, with monitoring equipment installed 7 meters from the working face, as illustrated in Figure 9.

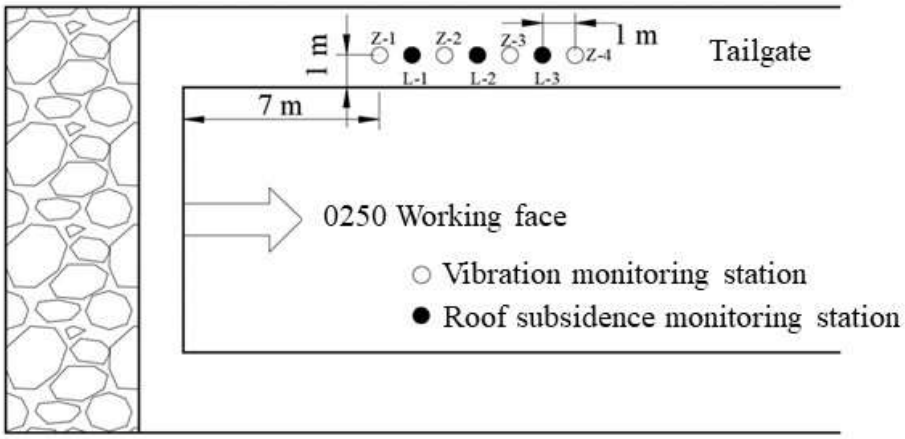

(a)

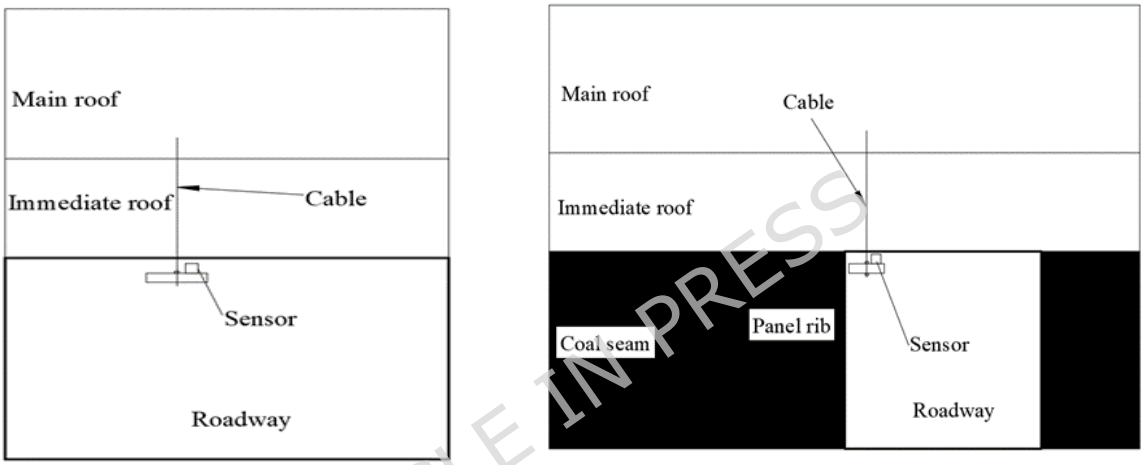

(b) (c)

Figure 9. Monitoring deployment of 0250 working face. (a) vertical view. (b) Front view. (c) Side view.

Four vibration measurement points, designated Z1 through Z4, and three roof subsidence measurement points, labeled L1 through L3, are positioned 1 meter apart. Roof drilling occurs 1 meter from the rib on the mining side of the roadway. The installation depth of the holes ranges from 6 to 7 meters, with the cable anchored into the main roof. A U-shaped buckle secures the tray and nut at the cable's end. The vibration sensor is affixed to the cable tray using cement (Fig. 9b). According to the instrument manual, engineering vibration frequencies typically range around 100 Hz. To ensure comprehensive signal acquisition while minimizing interference from high-frequency noise, the sampling frequency should be set between 10 and 100 times the signal frequency, specifically between 1 kHz and 10 kHz. This strategy necessitates collecting 10 to 100 samples per vibration cycle to prevent distortion of the measurement signal waveform. For routine vibration testing with this equipment, sampling rates of 8 kHz or 16 kHz are recommended. In this experiment, the acquisition rate was established at 8 kHz. During coal bump events, the movement velocity of coal and rock masses can exceed 1 m/s, while roof subsidence rates during mining operations do not surpass 50 mm/day, even during the periodic pressure phase. This field test aims to verify the vertical movement of the roof in a mine susceptible to coal bumps. Therefore, this value can be regarded as an interval. The trigger threshold must exceed the sampling accuracy and

demonstrate a clear distinction from conventional mining pressure activities. Consequently, the vibration meter trigger threshold is set at 0.2 cm/s, with a fixed recording duration of 5 seconds.

Monitoring will commence at 00:00 on June 27, 2020, and conclude at 16:30 on June 28, 2020. The initial distances from the four measuring points to the mining face are 7 meters, 9 meters, 11 meters, and 13 meters, respectively. The Ionometer installation will begin at 18:00 on June 26, 2020. The distances from the three measuring points to the working face are 8 meters, 10 meters, and 12 meters. The drilling depths are 6.8 meters, 6.7 meters, and 6.7 meters, with the number of embedded anchor points being 13, 11, and 11, respectively.

Monitoring commenced at 0:00 on June 27, 2020, and concluded at 2:45 on June 29, 2020. The Ionometer records data per cut, with each measurement point capturing 11 data points, resulting in a total of 33 recorded data points.

Figure 10 shows the data comparison chart for Z1 to Z4. As illustrated in Figure 10, the vertical velocity variations at the roof of the advancing working face display discrete and random characteristics as the face progresses. Regarding the temporal distribution of the collected data, a substantial proportion is concentrated between 00:00 and 14:00 each day. The box plot indicates that on the first day, data from all four vibration sensors were predominantly clustered between 1 cm/s and 5 cm/s, whereas on the second day, the measurements primarily ranged from 1 cm/s to 15 cm/s.

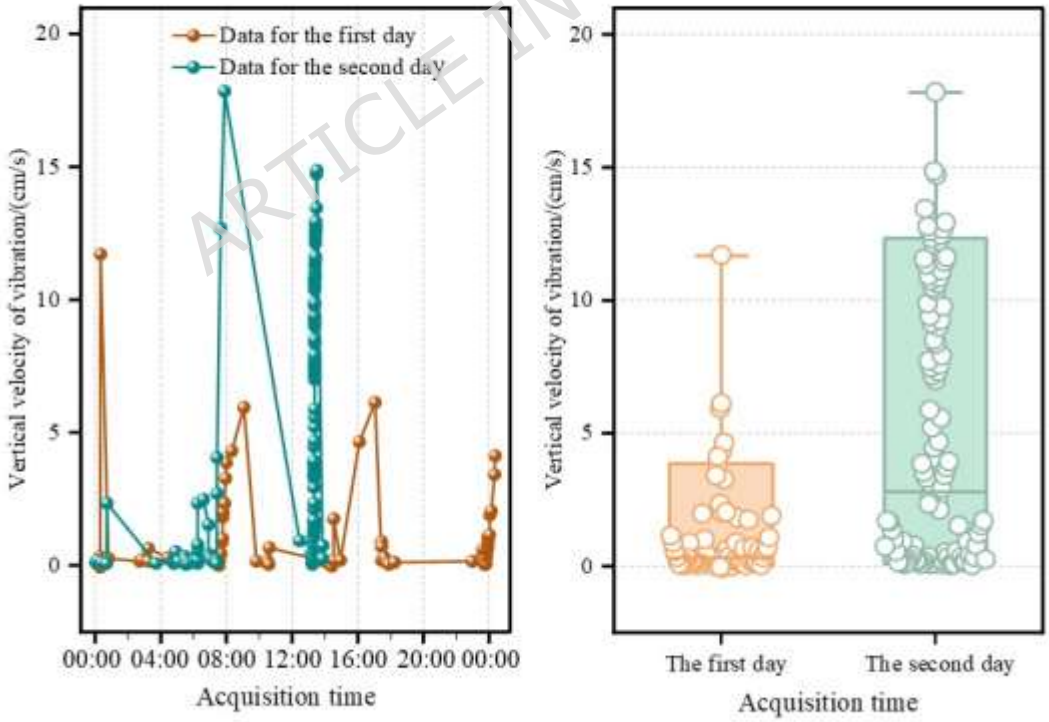

(a) Z1 data

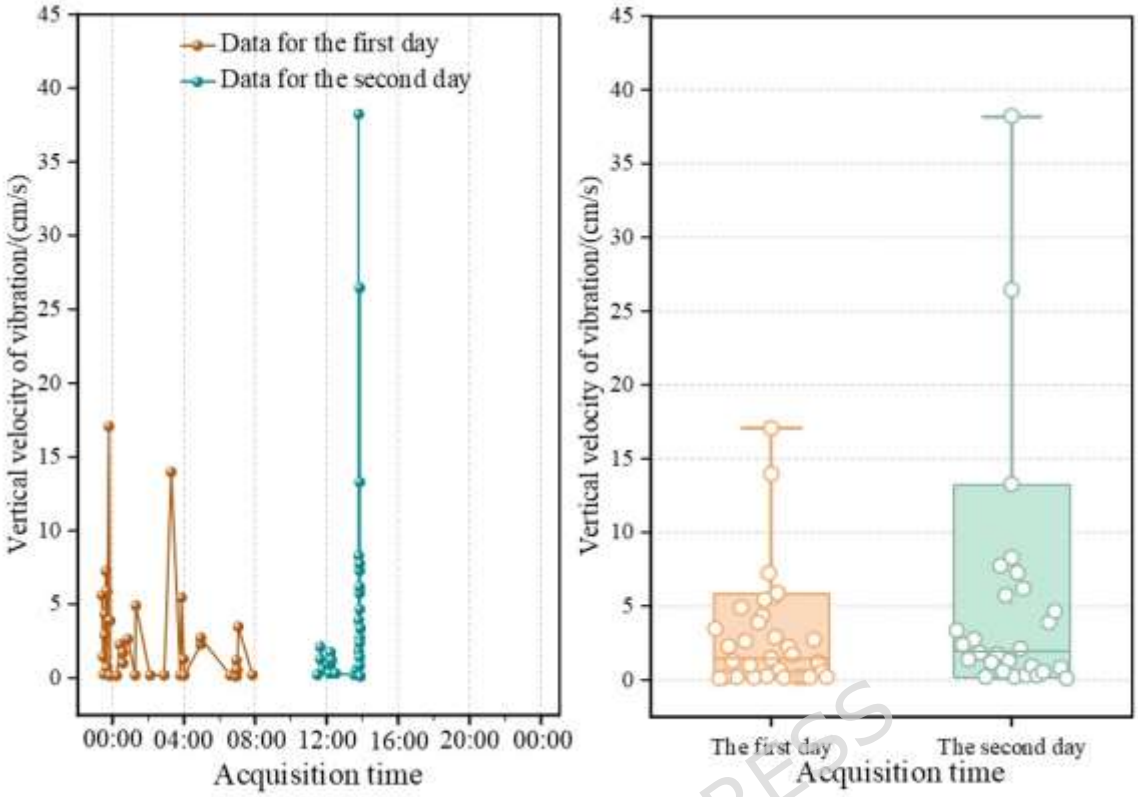

(b) Z2 data

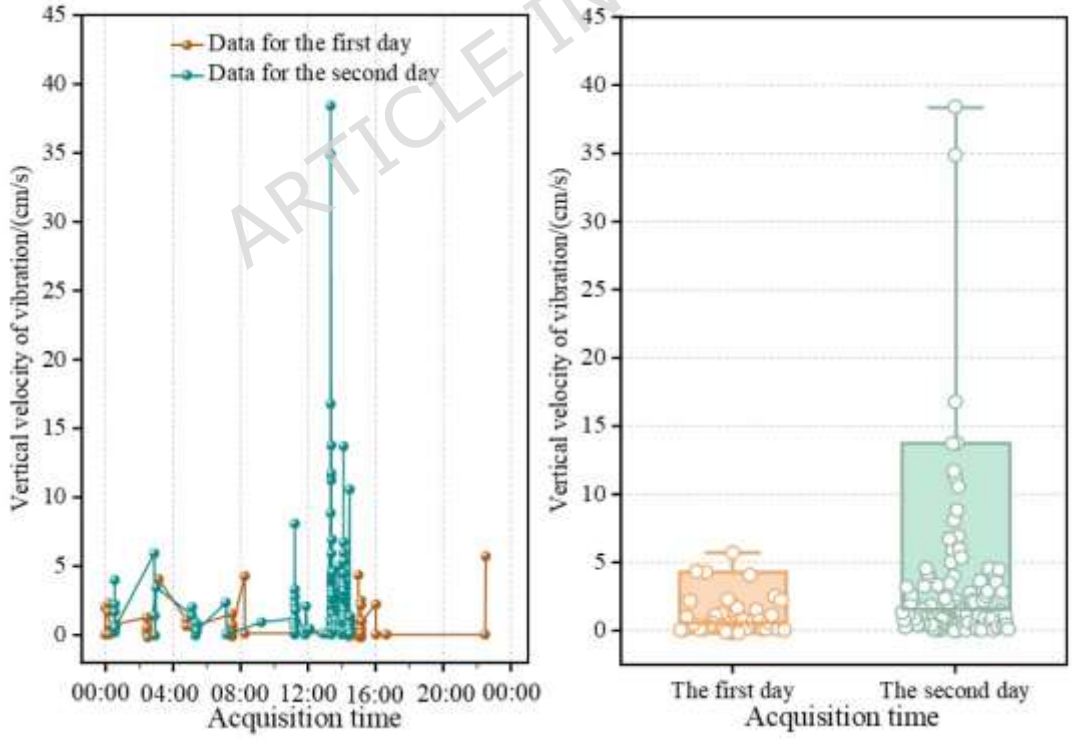

(c) Z3 data

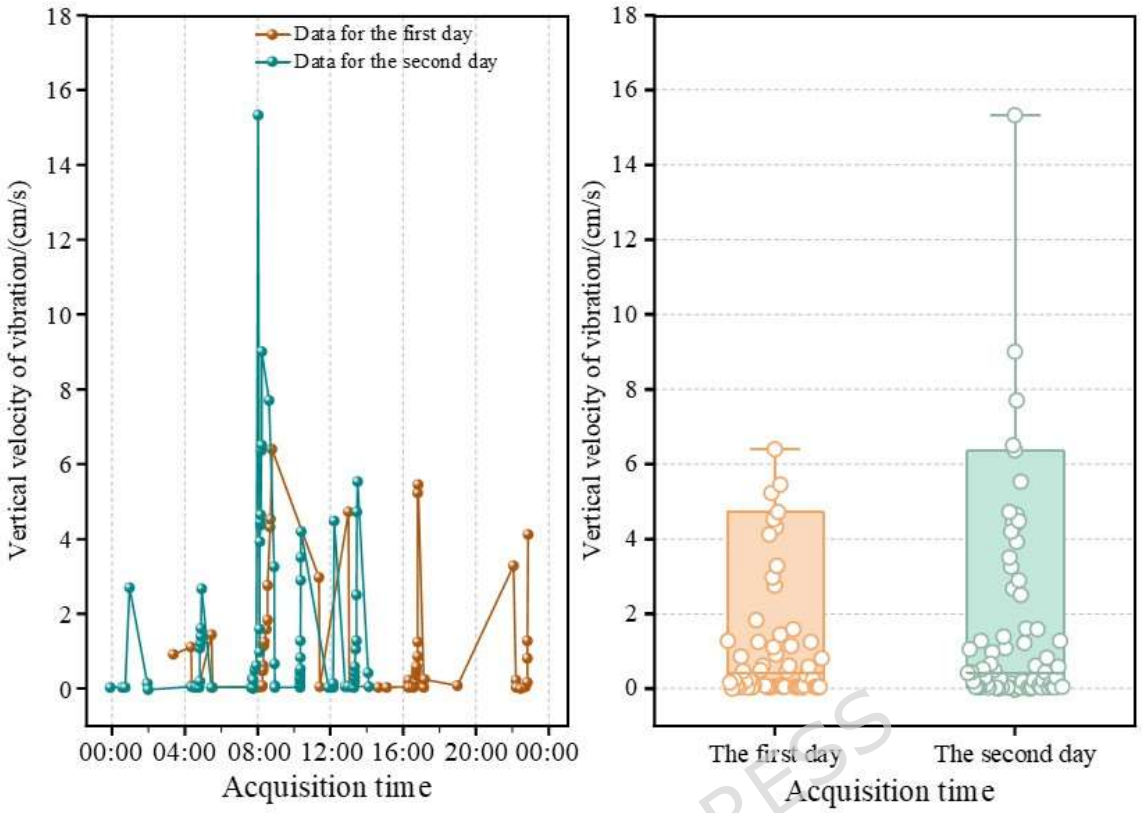

(d) Z4 data

Figure 10. Vertical velocity relation of roof vibration

6 Results and analysis

6.1 Roof vibration

The monitoring time of roof vibration is from 0:00 on June 27, 2020 to 16:30 on June 28, 2020, during which the working face is advanced by 4 m. More than 1900 data were obtained after the monitoring. Environmental factors may cause signal waveforms to superimpose interference signals. The Blasting Vibration Analysis software (BVA), used in conjunction with the TC-4850 Blasting Vibration Analyzer, processes collected data, including filtering analysis. Engineering vibration frequencies typically fall within the low-frequency range around 100Hz. Therefore, during this application, a “low-pass filter” was employed to eliminate high-frequency signals while preserving the low-frequency components. The data are processed and the vibration wave curves are obtained. Because the dynamic load monitoring only aims at the vertical movement of the roof, these data are screened to get the vertical movement. The typical vertical vibration velocity curve is shown in Figure 11.

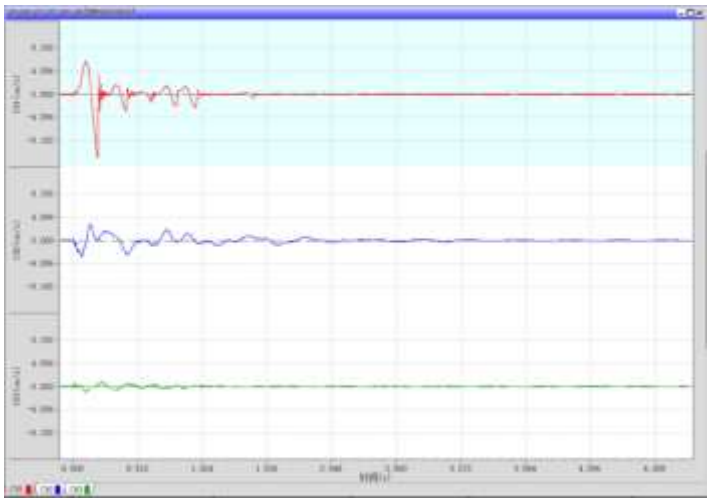

Figure 11. Typical vibration velocity curve.

By comparing the data, the maximum vertical velocity distribution from four sensors over two days was obtained, as illustrated in Figure 12.

The maximum vertical velocity of roof vibration is typically observed to range from 2 to 15 cm/s, which is lower than the horizontal velocity. Each vibration event exhibited a short duration (1–2 s), consistent with dynamic disturbances associated with mining activities. The active period of roof vibration occurs daily around 0 and 13 o'clock, corresponding to the initiation and cessation of mining operations.

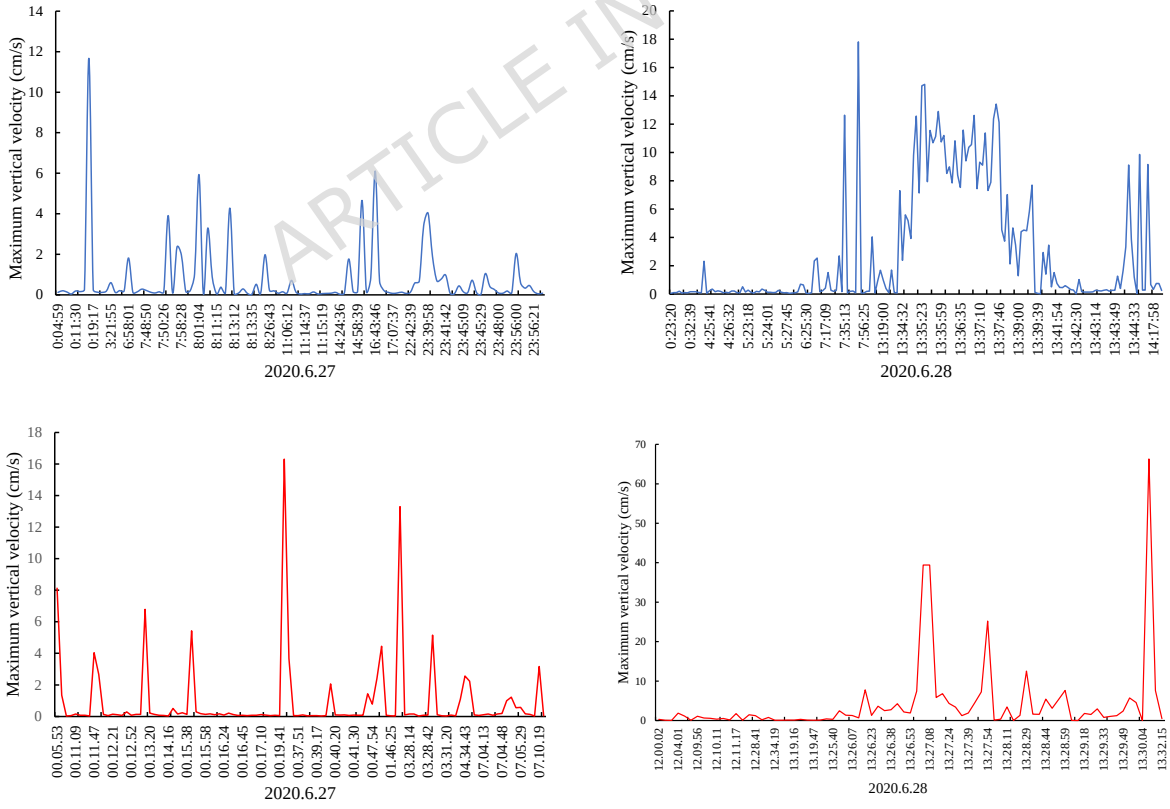

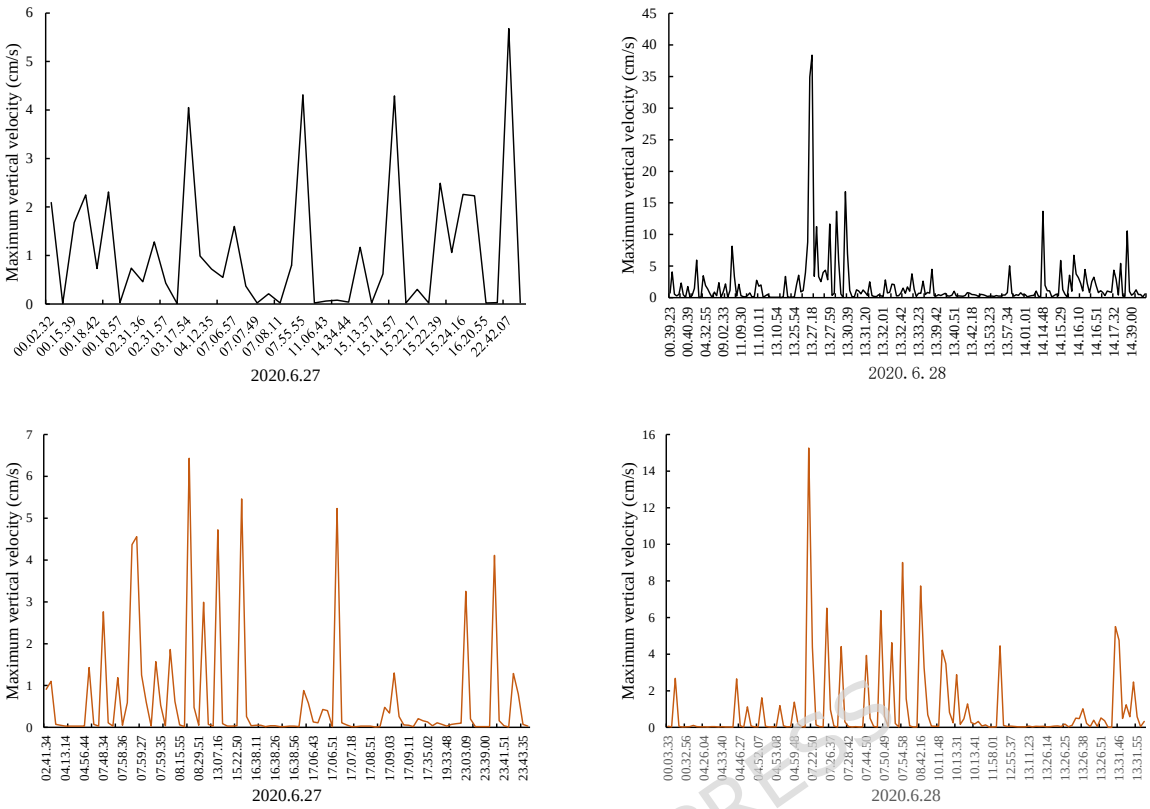

Figure 12. Maximum vertical velocity distribution, from top to bottom Z1-Z4

6.2 Roof subsidence

The monitoring period for roof subsidence spans from June 27, 2020, to June 29, 2020, during which the working face advanced by 5 m. The displacement variation diagram for a typical anchor point is presented in Figure 13.

The first anchor point serves as the reference point for calculating the relative displacements of other measurement points during the advancement of the working face. The results are illustrated in Figure 14.

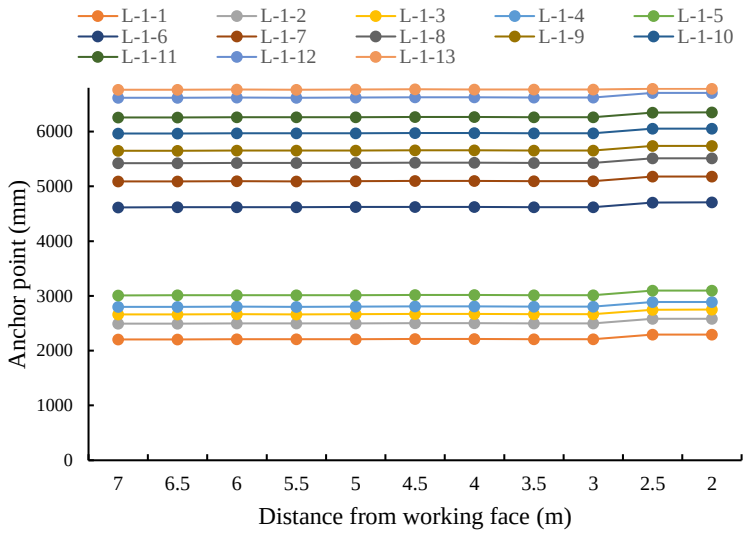

Figure 13. Typical anchor point movement.

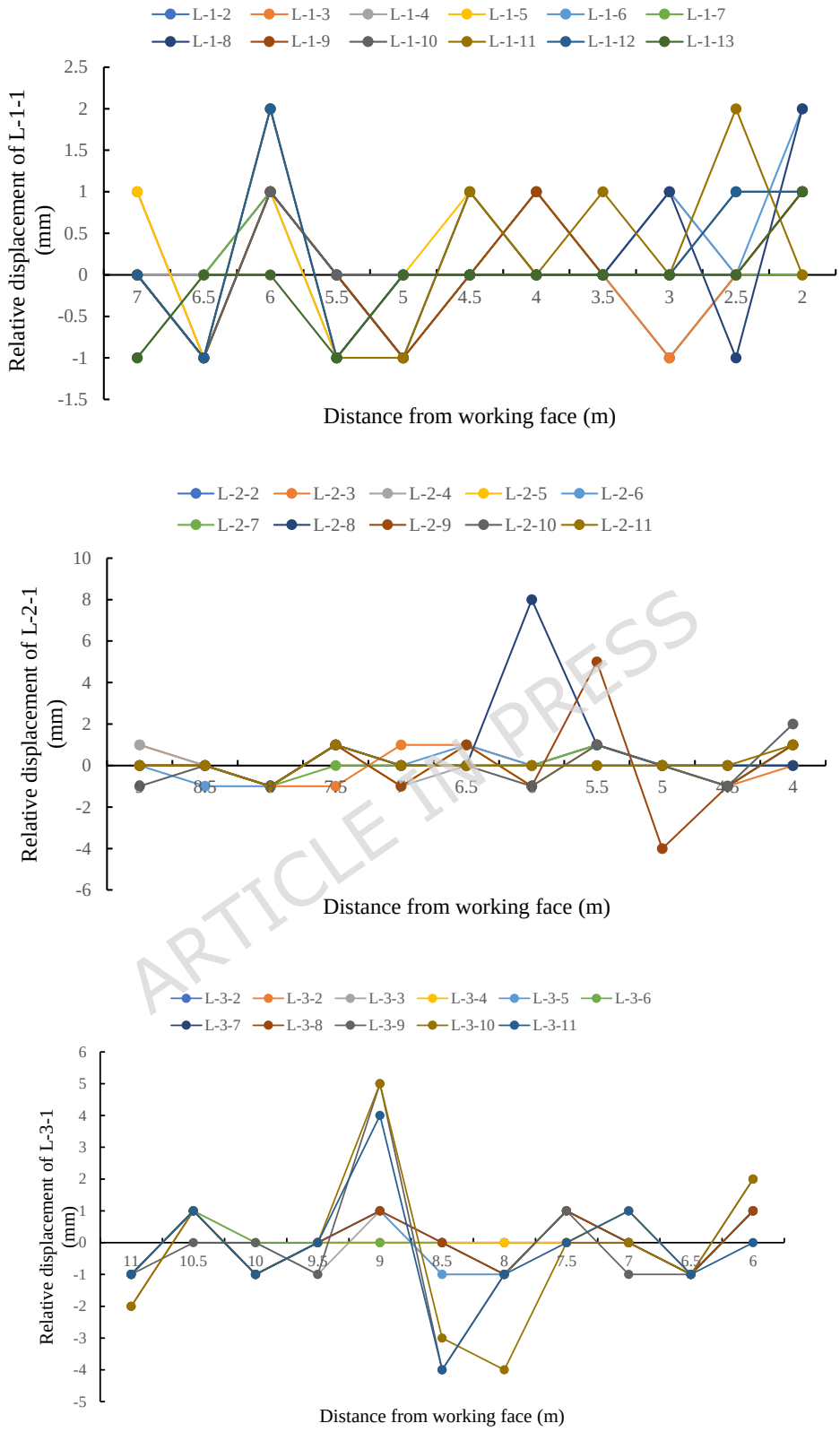

Figure 14. The relative displacement of each anchor point.

The results indicate that the relative displacement at each point within the three measurement holes is minimal, with only slight changes observed. When L1 is positioned 3 m from the working face, the

measured values at each anchor point exhibit a slight increase, suggesting roof rebounding. Notably, the relative movement among the anchor points varies as the mining face progresses.

6.3 Roof Vertical displacement analysis

More than 700 data points were collected from roof vibration monitoring. After data screening, 96 vertical vibration-induced data points were retained. Blasting Vibration Analysis (BVA) software, specifically designed for the TC-4850 Blasting Vibration Meter, facilitates direct integration calculations. The operational steps for the software are as follows: 1) Open a data file and select the menu item Analysis First-Order Differentiation/Integration to access an auxiliary window beneath the main time-domain window. 2) Adjust the waveform curve by resizing and repositioning it using the toolbar located at the top of the interface. 3) Close the differentiation/integration window by double-clicking the "Auxiliary Window" button with the left mouse button to exit the interface. The vertical displacement of the roof was calculated by integrating each velocity data over time. The results are presented in Figure 15, where the 1st, 2nd, and 3rd series correspond to three distinct data collection instances.

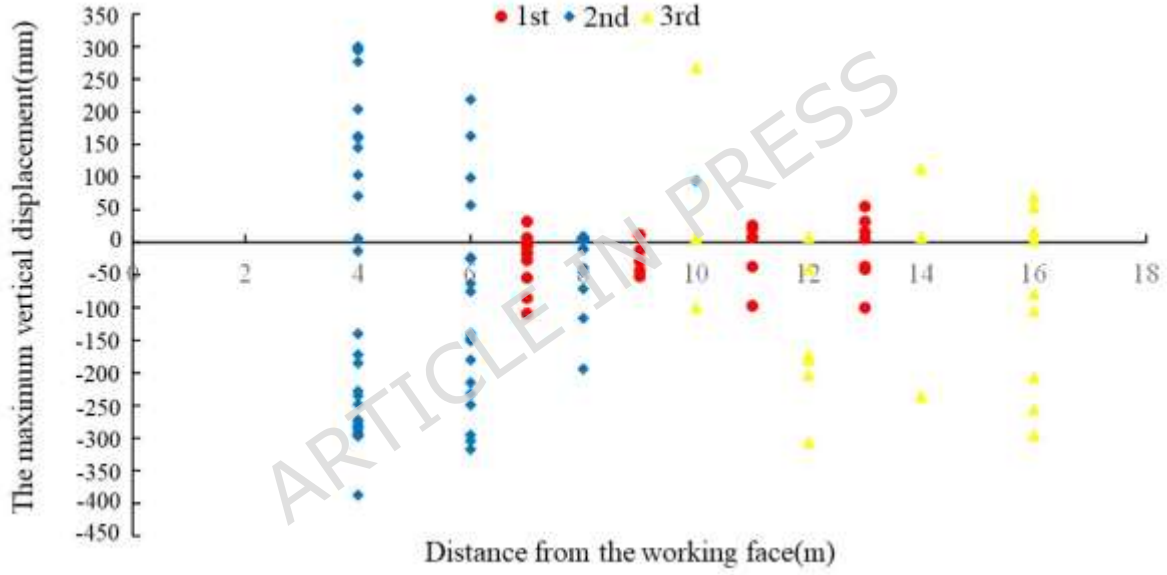

Figure 15. The vertical displacement of the roof.

The results indicate that the maximum vertical displacement of roof vibration is approximately ± 350 mm, occurring in an area 4-6 m in advance of the working face. Given the proximity of this area to the working face, it is reasonable to conclude that the vibration is associated with coal cutting and the movement of hydraulic supports. Engineering experience suggests that the region 4-6 m ahead of the working face is not a primary site for coal bumps. Consequently, it can be inferred that the roof vibration in this area reflects the overall movement of the surrounding rock, making it unlikely to trigger a coal bump.

The section 7-16 m in advance of the working face is characterized by high abutment pressure, and the impact of dynamic disturbances in this area constitutes the primary focus of the dynamic disturbance analysis. Monitoring results indicate that the maximum roof displacement is within ± 100 mm. In working

faces with a high propensity for coal bumps, the vertical displacement of the working face may exceed 200 mm. Drawing on the experiences from similar working faces, it can be concluded that the roof displacement at the 0250 working face is within acceptable limits.

The preceding analysis yields several conclusions. Coal blasting and pressure relief drilling partially release the accumulated elastic energy within the coal seam, which is essential for seam mining. During the mining process, monitoring and analysis of dynamic load data reveal that the relative displacement of the roof is minimal, indicating its structural integrity. Additionally, the vertical displacement data of the roof demonstrate that vibrations near the working face primarily result from coal cutting and hydraulic shield movement, suggesting a very low likelihood of inducing a coal bump. In the high abutment pressure zone (7–16 m ahead), the monitored vertical displacement remained within ±100 mm, indicating that the pressure-relief measures effectively reduced the elastic energy concentration. The conclusion is that 0250 working face can be safely mined.

7 Problems and Prospects

The vibration meter is primarily utilized in the machinery industry and for slope monitoring. Due to the brief duration of explosion waves, the monitoring period of the instrument is consequently limited. In the context of dynamic load monitoring in underground coal mines, the extended monitoring period necessitates modifications to the equipment. Furthermore, the instrument generates a substantial volume of data, complicating the data processing requirements. Therefore, it is essential to develop automated processing software to meet the demands for rapid monitoring in underground coal mines.

This study focuses on monitoring the movement of the cable end, necessitating an examination of the coupling relationship between the cable end and roof displacement to mitigate errors arising from discrepancies in their respective displacements.

The vibration instrument is capable of directly monitoring both the velocity and displacement of the roof, indicating significant potential for future applications in dynamic load monitoring and coal bump prediction.

8 Conclusion

In light of the re-establishment of the 0250 working face following the coal bump disaster at the Tangshan coal mine, pressure relief measures prior to mining and dynamic load monitoring during the mining process were implemented. The following conclusions can be drawn:

(1) Coal blasting and pressure relief drilling can alleviate a portion of the accumulated elastic energy within the coal mass, thereby effectively reducing the likelihood of a coal bump.

(2) Monitoring results for roof vibration and separation indicate that, following the implementation of pressure relief measures, the influence of dynamic loads on the 0250 working face is manageable, thereby facilitating safe production operations.

(3) Challenges including intermittent monitoring and external environmental interference in roof separation and vibration assessments necessitate further optimization of the analysis of monitoring results.

Data Availability

All data of this article has been included in this manuscript.

References

1. Gao, M. T., Song, Z. Q., Duan, H. Q., Xin, H. Q. & Tang, J. Q. Mechanical Properties and Control Rockburst Mechanism of Coal and Rock Mass with Bursting Liability in Deep Mining. *Shock Vib.*2020, 8833863 (2020). https://doi.org/10.1155/2020/8833863.
2. Wang, Z. S., Liu, Y. L., Song, Z. X., Cong, L. & Zhu, Y. T. Rockburst mechanism and prevention technology for wide coal pillar return airway. *Energy Sci. Eng.*2024, **12,** 4991–5007 (2024). https://doi.org/10.1002/ese3.1922.
3. Chen, B. Stress-induced trend: the clustering feature of coal mine disasters and earthquakes in China. *Int. J. Coal Sci. Technol.* 2020, **7,** 334–352 (2020). https://doi.org/10.1007/s40789-020-00334-z.
4. Cao, D. Y., Wang, A. M., Ning, S. Z., Li, H. T., Guo, A. J., Chen, L. M., Liu, K., Tan, J. Q. & Zheng, Z. H. Coalfield structure and structural controls on coal in China. *Int. J. Coal Sci. Technol.* 2020, **7,** 310–333 (2020). https://doi.org/10.1007/s40789-020-00326-z.
5. Mao, S. J. Development of coal geological information technologies in China. *Int. J. Coal Sci. Technol.* 2020, **7,** 320–328 (2020). https://doi.org/10.1007/s40789-020-00340-1.
6. Lian, X. G., Hu, H. F., Li, T. & Hu, D. S. Main geological and mining factors affecting ground cracks induced by underground coal mining in Shanxi Province, China. *Int. J. Coal Sci. Technol.* 2020, **7,** 353–368 (2020). https://doi.org/10.1007/s40789-020-00308-1.
7. Wu, X., Peng, Y. W., Xu, J., Yan, Q., Nie, W. & Zhang, T. T. Experimental study on evolution law for particle breakage during coal and gas outburst. *Int. J. Coal Sci. Technol.* 2019, **6,** 267–278 (2019). https://doi.org/10.1007/s40789-019-00284-1.
8. Małkowski, P., Niedbalski, Z. & Balarabe, T. A statistical analysis of geomechanical data and its effect on rock mass numerical modeling: a case study. *Int. J. Coal Sci. Technol.* 2020, **7,** 409–425 (2020). https://doi.org/10.1007/s40789-020-00369-2.
9. Wang, X. H. Research on the influence mechanism of tectonic stress in the “three hard” coal seam in coalfield on rockbursts. *Chem. Technol. Fuels Oils* 2023, **59,** 1048–1057 (2023). https://doi.org/10.1007/s10553-023-01617-2.
10. Tian, H. M., Chen, W. Z., Ma, C. S., Yang, D. S. & Tan, X. J. Energy Release Analysis of a Severe Rockburst in a Headrace Tunnel Crossing a Tectonic Stress Zone. *Shock Vib.* 2019, 8959845 (2019). https://doi.org/10.1155/2019/8959845.
11. Xue, D. J., Lu, L., Zhou, J., Lu, L. & Liu, Y. T. Cluster modeling of the short-range correlation of acoustically emitted scattering signals. *Int. J. Coal Sci. Technol.* 2020, **7,** 387–408 (2020). https://doi.org/10.1007/s40789-020-00357-6.
12. Xue, D. J., Zhou, J., Liu, Y. T. & Gao, L. On the excavation-induced stress drop in damaged coal considering a coupled yield and failure criterion. *Int. J. Coal Sci. Technol.* 2020, **7,** 369–386 (2020). https://doi.org/10.1007/s40789-020-00299-z.

13. Liu, X. Q., Wang, G., Song, L. B., Han, G. S., Chen, W. Z. & Chen, H. A new rockburst criterion of stress–strength ratio considering stress distribution of surrounding rock. *Bull. Eng. Geol. Environ*. 2023, **82,** 29 (2023).https://doi.org/10.1007/s10064-022-03042-x.
14. Wang, S. W., Cao, A. Y., Wang, C. B., Guo, W. H., Xue, C. C., Liu, J. G., Wu, X. S. & Shi, G. S. Mechanism of rockburst induced by the microseismic event in the floor strata of high tectonic stress zones: A case study. *Int. J. Coal Sci. Technol.* 2024, **11,** 76 (2024). https://doi.org/10.1007/s40789-024-00728-3.
15. Wang, S. R., Wang, Y. H., Gong, J., Wang, Z. L., Huang, Q. X. & Kong, F. L. Failure mechanism and constitutive relation for an anchorage segment of an anchor cable under pull-out loading. *Acta Mech.* 2020, https://doi.org/10.1007/s00707-020-02717-4 (2020).
16. Zhang, L., Li, J. H., Xue, J. H., Zhang, C. & Fang, X. Q. Experimental studies on the changing characteristics of the gas flow capacity on bituminous coal in CO_2-ECBM and N_2-ECBM. *Fuel* 2021, **291,** 120115 (2021). https://doi.org/10.1016/j.fuel.2020.120115.
17. Lin, J., Ren, T., Cheng, Y., Nemcik, J. & Wang, G. Cyclic N_2 injection for enhanced coal seam gas recovery: A laboratory study. *Energy* 188, 116115(2019).https://doi.org/10.1016/j.energy.2019.116115.
18. Zhang, J. W., Bai, X. Y., Song, Z. X., Zhang, Y., Dong, X. K., Wu, S. K., Xing, C. R., Li, X., Xu, W. Z. & Zhang, S. L. Research Progress and Perspectives on Prevention and Control Technologies for Coal–Rock–Gas Composite Dynamic Disasters: New Types of Induced Classifications, Discriminant Criteria, and Structural Control Schemes. *Rock Mech. Rock Eng*. 2025, https://doi.org/10.1007/s00603-025-04657-8.
19. Gong, F. Q., Dai, J. H. & Xu, L. A strength-stress coupling criterion for rockburst: Inspirations from 1114 rockburst cases in 197 underground rock projects. *Tunn. Undergr. Space Technol.* **142,** 105396 (2023). https://doi.org/10.1016/j.tust.2023.105396.
20. Ma, Z., Li, S. & Zhao, X. Energy Accumulation Characteristics and Induced Rockburst Mechanism of Roadway Surrounding Rock under Multiple Mining Disturbances: A Case Study. *Sustainability* **15,** 9595 (2023). https://doi.org/10.3390/su15129595.
21. Xuan, Z., Cheng, Z., Li, C. *et al*. Energy evolution mechanism during rockburst development in structures of surrounding rocks of deep rockburst-prone roadways in coal mines. *Front. Energy Res.* **11,** 1283079 (2023). https://doi.org/10.3389/fenrg.2023.1283079.
22. Xue, D. J., Liu, Y. T., Zhou, H. W., Wang, J. Q., Liu, J. F. & Zhou, J. Fractal Characterization on Anisotropy and Fractal Reconstruction of Rough Surface of Granite Under Orthogonal Shear. *Rock Mech. Rock Eng.* 2019, https://doi.org/10.1007/s00603-019-01974-7.
23. Du, K., Bi, R. Y., Khandelwal, M., Li, G. C. & Zhou, J. Occurrence mechanism and prevention technology of rockburst, coal bump and mine earthquake in deep mining. Geomech. Geophys. Geo-energ. Geo-resour. 2024, **10,** 98 (2024). https://doi.org/10.1007/s40948-024-00768-8.
24. Mi, C. N., Zuo, J. P., Sun, Y. J. & Zhao, S. K. Investigation on Rockburst Mechanism Due to Inclined Coal Seam Combined Mining and its Control by Reducing Stress Concentration. *Nat. Resour. Res*. 2022, **31,** 3341–3364 (2022). https://doi.org/10.1007/s11053-022-10118-8.

25. Du, F., Ma, J., Guo, X. F., Wang, T. F., Dong, X. H., Li, J. S., He, S. L. & Nuerjuma, D. Rockburst mechanism and the law of energy accumulation and release in mining roadway: a case study. *Int. J. Coal Sci. Technol.* 2022, 9, 67 (2022). https://doi.org/10.1007/s40789-022-00521-0.

Acknowledgments

This work was supported by the Doctoral Scientific Research Foundation of Liaoning Province (2025-BS-0395), and the University-local Government Scientific and Technical Cooperation Cultivation Project of Ordos Institute-LNTU(YJY-XD-2023-18). These supports are gratefully acknowledged. The authors are grateful to the reviewers for discerning comments on this paper.

Author Contributions

Y.S.: Drafting the manuscript, accident analysis , data organization and collection, plotting diagrams and tables and responding to reviewers.

S.M.: Drafting—reviewing and editing, accident analysis, validation, project management, overseeing the research findings.

D.J.: Data organization and collection.

X.W.: Analyzing the accident.

G.L.: Participating in the design charts.

B.G.: Participating in the design charts.

H.L.: Participating in the research guidance and paper revision for this thesis.

T.W.: Analyzing the accident.

All authors discussed the paper's results.

Conflicts of Interest

The authors declare that there is no conflict of interest regarding the publication of this paper.

Funding

Doctoral Scientific Research Foundation of Liaoning Province (2025-BS-0395) and University-local Government Scientific and Technical Cooperation Cultivation Project of Ordos Institute-LNTU(YJY-XD-2023-18).

Additional information

Correspondence and requests for materials should be addressed to S.M